# DECOUPLING PILOT BIOMECHANICS FROM CONTROL DEVICE DYNAMICS IN BIODYNAMIC FEEDTHROUGH: A MULTIBODY DYNAMICS APPROACH

C. Talamo*,◇, A. Zanoni◇, T. Aresi◇, P. Masarati◇ E. Fosco† F. Colombo†

◇Politecnico di Milano - Dipartimento di Scienze e Tecnologie Aerospaziali, Campus Bovisa, Via La Masa 34, 20156 Milano, Italy

†Leonardo Helicopter Division, Cascina Costa di Samarate, 21017, VA, Italy

* e-mail: carmen.talamo@polimi.it

**Abstract**

In human-vehicle interaction, particularly Rotorcraft-Pilot Couplings (RPCs), the Biodynamic Feedthrough (BDFT) assesses the vibration transmission from the base to the control device. In rotorcraft, BDFT is represented as a transfer function, $H_{\text{BDFT}}$, detailing the relationship between seat acceleration and inadvertent control device motion. However, $H_{\text{BDFT}}$ depends on both pilot and control device dynamics, challenging design engineers aiming to mitigate RPC impacts on vehicle handling. In this study, a decomposition of $H_{\text{BDFT}}$ into separate pilot and control device contributions is assessed using both numerical and experimental approaches. The computational procedure includes a multibody model of the upper body and collective lever, while tests are conducted with specialized setup and the support of the RPC testbed at Politecnico di Milano. Both methods proved effective, validating the approach. This work sets the stage for future research involving diverse individuals to test the model's predictive capabilities and perform sensitivity analysis, supporting robust helicopter flight control system development.

## 1 Introduction

In the domain of human-vehicle interaction, particularly within the realm of Rotorcraft-Pilot Couplings (RPCs) [1], the Biodynamic Feedthrough (BDFT), stands as a crucial metric for assessing the transmissibility of vibrations from the base - typically the seat - to the control device [2]. In rotorcraft, this measure is commonly articulated as a transfer function delineating the correlation between seat acceleration and the consequent inadvertent motion of the control device, denoted as the Biodynamic Feedthrough to positions (B2P), or $H_{B2P}$, following the nomenclature proposed by Venrooij [2] (In this work, $H_{B2P}$ will be referred to with the more general notation $H_{\text{BDFT}}$). $H_{\text{BDFT}}$ proves very useful in evaluating the influence of pilot biodynamic responses on the closed-loop stability of the pilot-vehicle system.

Nevertheless, the Biodynamic Feedthrough to positions exhibits a notable drawback: its nature as a function dependent on both pilot and control device dynamics, both contributing to the overall vibration transmissibility. For design engineers tasked with crafting the flight control system for a novel aircraft or retrofitting an existing one to alleviate the impact of RPCs on vehicle handling qualities, this poses a significant limitation. Design engineers aspire to identify and differentiate between potential adverse interactions, discerning those modifiable through interventions in the flight control system from those inherent to pilot biomechanics, which cannot be readily altered. In conceptual terms, the former constitute design variables, while the latter present as constraints, mandating robustness.

Separating the components of the BDFT experimentally can be quite challenging, especially if time and cost requirements mandate the simultaneous identification of the pilot and vehicle contributions [3]. On the other hand, it is possible to notice that the pilot contributions, showing a strong dependence on muscular activity, is subjected to a significant stochastic variation, while components related to the control device are far more deterministic. For this reason and more, an appealing approach to the problem is represented by the use of numerical multibody models of pilot and control device, that can be utilized in evaluating the different components of the BDFT and assessing the sensitivity of it with respect to the driving parameters of the pilot biomechanics and the control device servomechanical properties.

## 2 Research Goals

Given a global definition of the BDFT:

$$H_{\text{BDFT}}(s) = \frac{\theta_{\text{cd}}(s)}{a_{\text{dist}}(s)} \tag{1}$$

where $\theta_{\text{cd}}(s)$ is the deflection of the control device, while $a_{\text{dist}}$ is the acceleration (disturbance) of the cockpit, measured at the pilot's seat, the following research questions will be addressed:

I is it possible to robustly separate the BDFT components related to the pilot from those related to the lever?



Presented at the 50th European Rotorcraft Forum, Marseille, France, 10–12 September, 2024

II can this decomposition be consistently and efficiently achieved using a detailed numerical model of the lever and pilot?

III which are the experimental setup and procedures necessary to validate such process?

# 3 Methods

The design and the results of a series of numerical tests conducted on a multibody model incorporating human upper body biomechanics (head, spine, upper limbs) and conventional helicopter control devices (collective and cyclic levers) [4] will be presented, along with the design, implementation and results of experimental tests dedicated to the validation of the numerical models.

The focus is directed towards the collective axis, therefore $\theta_{\text{cd}}$ appearing in equation (1) is representing the collective lever deflection, while $a_{\text{dist}}$ is representing the seat acceleration in the heave direction.

The tests aim to identify the components of the rotorcraft-pilot biodynamic feedthrough, following the conceptual schematics first proposed by Venrooij [2]. The transfer function $H_{\text{BDFT}}$ can be viewed as the composition of four distinct elements (Cf. Figure1):

$$H_{\text{BDFT}}(s) = \frac{\theta_{\text{cd}}(s)}{a_{\text{dist}}(s)} = \frac{H_{\text{ADM}} H_{\text{CD}}}{H_{\text{ADM}} - H_{\text{CD}}} \left(H_{\text{B2FOL}} + H_{\text{CDFT}}\right) \tag{2}$$

Each component has the following meaning:

- $H_{\text{CD}} = \frac{\theta_{\text{cd}}(s)}{T_{\text{tot}}(s)}$: the **control device dynamics**, i.e. the control deflection $\theta_{\text{cd}}$ as a function of a torque $T_{\text{tot}}$ directly applied to it, with the base fixed ($a_{\text{dist}} = 0$) and the pilot detached from the lever;

- $H_{\text{CDFT}} = \frac{T_{\text{cdft}}(s)}{a_{\text{dist}}(s)}$: the **control device feedthrough**, i.e. the moment generated on the control lever as a function of the base acceleration, with the pilot detached from the lever;

- $H_{\text{ADM}} = \frac{\theta_{\text{cd}}(s)}{T_{\text{nms}}(s)}$: the **neuromuscular admittance**, i.e. the rotation of the control device due *only* to the action of the pilot biomechanics, with the base fixed;

- $H_{\text{B2FOL}} = \frac{T_{\text{b2fol}}(s)}{a_{\text{dist}}(s)}$: the **biodynamic feedthrough to force in open loop**, i.e. the torque generated on the control device by the pilot biomechanics, as a function of the base acceleration, with the control device fixed.

Notice that the neuromuscular admittance is, by definition [2], only a function of the pilot biomechanics. Therefore $T_{\text{nms}}$ is the moment generated by the reaction forces and moments exchanged between the pilot's hand and the control lever.

In general terms, the first two blocks, $H_{\text{CD}}$ and $H_{\text{CDFT}}$, exclusively pertain to the control device, whereas $H_{\text{ADM}}$ and $H_{\text{B2FOL}}$ are solely determined by pilot biomechanics.

It is also possible to define the combination of the control device dynamics $H_{\text{CD}}$ and the neuromuscular admittance, $H_{\text{ADM}}$, the **force dynamics feedthrough**, $H_{\text{FDFT}}$:

$$H_{\text{FDFT}} = \frac{\theta_{\text{cd}}(s)}{T_{\text{dist}}(s)} \tag{3}$$

which represents the input-output relationship between the rotation of the control device and the torque applied to it, with the pilot holding the lever. It is important to notice that the knowledge of $H_{\text{FDFT}}$ allows to recover $H_{\text{ADM}}$, which can be difficult to measure directly in practice[5], from the knowledge of $H_{\text{CD}}$:

$$H_{\text{FDFT}} = \frac{H_{\text{ADM}} H_{\text{CD}}}{H_{\text{ADM}} - H_{\text{CD}}} \tag{4}$$

.

Furthermore, it is possible to notice that $H_{\text{CDFT}}$ assumes a particularly simple shape. In fact, considering a Linear Time-Invariant (LTI) model of the control device, forced by the base vertical acceleration:

$$J_\ell \ddot{\theta} + c_\ell \dot{\theta} + (k_\ell - S_\ell g)\theta = -S_\ell \cos\theta_0 \ddot{z}(t) \tag{5}$$

where $J_\ell$ is the moment of inertia of the inceptor with respect to the pivot axis, $c_\ell$ and $k_\ell$ represent respectively the equivalent damping and the equivalent stiffness of the control chain elements, evaluated for the control lever rotation about the pivot axis, $S_e ll$ is the first moment of inertia of the inceptor (the product of its mass times the distance of the center of mass with respect to the pivot axis), $\theta_0$ is the static equilibrium position assumed by the control inceptor. The vertical acceleration of the base is $\ddot{z}(t)$. Considering that

$$T_{\text{cdft}} = J_\ell \ddot{\theta} + c_\ell \dot{\theta} + (k_\ell - S_\ell g)\theta \tag{6}$$

the control device feedthrough results simply in

$$H_{\text{CDFT}} = -S_\ell \cos\theta_0 \tag{7}$$

Four numerical tests are devised and conducted to identify the transfer functions of these components. Subsequently, the results from combining individual components to estimate $H_{\text{BDFT}}$ are compared against direct numerical tests, wherein the full model comprising both pilot and control devices is subjected to base acceleration, and the resulting collective rotation output is measured.

## 3.1 Multibody Dynamics

The numerical tests were performed using the general-purpose multibody dynamics analysis software MBDyn [6][1].

The complete pilot upper-body model (Figure 2) includes the spine (vertebrae and visceral masses), the torso (rib cage), the upper limbs (right and left arm), and the seat (cushion and backrest), along with a generic helicopter cockpit configuration (control inceptors and seat). The model is fully parameterized based on the age, sex, height, and weight of the pilot [7].

[1] https://www.mbdyn.org/

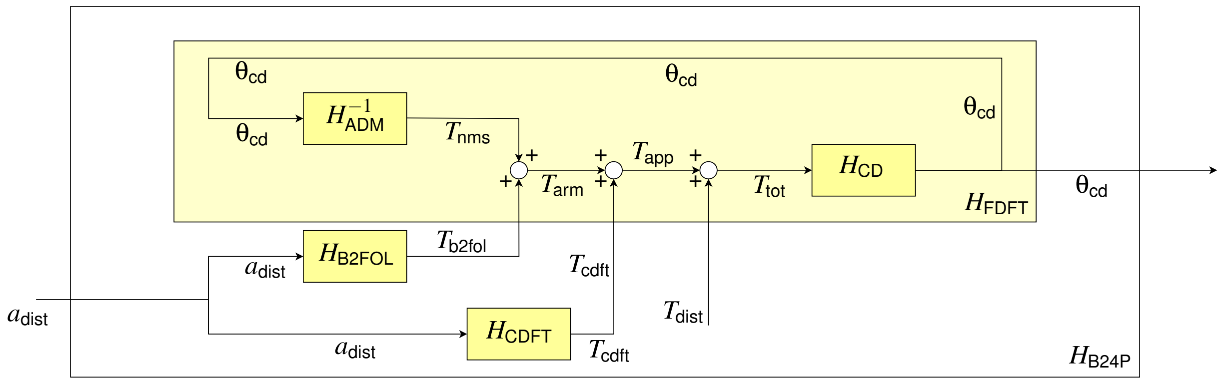


Figure 1: Block diagram highlighting the structure of the $H_{B2P}$.

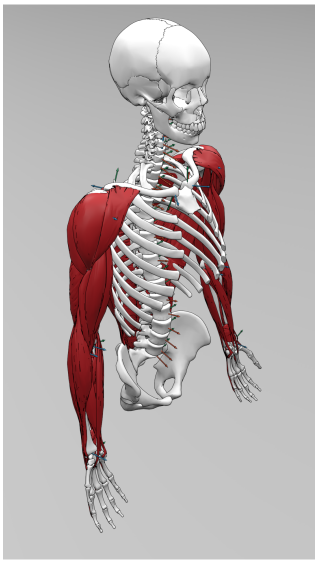

Figure 2: MBDyn Multibody Pilot Model

For the application here considered, which does not include poses of the upper limbs characterized by large shoulder abduction and flexion angles, the motion of the scapula and of the clavicle is neglected, and the humerus is directly joined to the torso with an ideal spherical joint. The remaining rigid bodies in the upper limbs model represent the radius, the ulna, and the hand of each limb. The hand is represented by a single rigid body.

The muscle forces are considered only tensile and depend on length, elongation rate, and muscle activation level. Specifically, each limb is actuated by 25 muscles, modeled by active viscoelastic 1-D elements. The force exerted by the $i$-th muscle is based on a modified version of the simplified Hill-type model originally proposed by Pennestr'i et al. in [8]. The dependencies of the force on the muscle peak isometric force, the elongation, and the elongation rate are developed as a function of three parameters: the peak isometric force ($f_0$), the reference length ($l_0$), and the reference velocity ($V_0$). These parameters can generally be set to a fixed value or as a function of $l_0$.

Once the non-dimensional length $x = l/l_0$ and velocity $v = \dot{l}/V_0$ are defined, the force due to the $i$-th muscle is expressed as:

$$f_{m_i} = f_0(f_1(x)f_2(v)a + f_3(x)), \tag{8}$$

where $f_3(x)$ is the passive contribution due to tendon elastic elements, while $f_1(x)$ and $f_2(v)$ are the active forces exerted by the muscles. Reference values for the parameters $l_0$ and $f_0$ can be found in [7], [9]. The parameter $a$ represents the muscle activation, with values between $0$ and $1$.

The value of $a$ is influenced by three contributions:

$$a(t) = a_0 + a_r(t) + a_{\text{TLAMs}}, \tag{9}$$

The reference activation $a_0$ is the minimum required to hold the reference static position and does not depend on time. The reflexive contribution $a_r(t)$ is defined as $a_r(t) = k_p(l - l_0) + k_d\dot{l}$, where $l$ is the muscle elongation. This represents the contribution aimed at maintaining the muscle's reference length and contractile velocity, often modulated by the pilot in an unconscious way. It is obtained through a quasi-steady approximation of the activation dynamics, likening the muscle control to a Proportional-Derivative (PD) controller.

Lastly, $a_{\text{TLAMS}}$ is the contribution from the simultaneous activation of antagonist muscles, which does not alter the torque generated by the muscle forces but changes the limb's equivalent impedance at the control inceptor. This contribution is introduced by the so-called Torque-Less Activation Modes (TLAMS), i.e. through combinations of activation that do not change the total resulting joint torques, as discussed in [7], [10].

The collective and cyclic inceptors are represented by rigid bodies as well, connected to the fixed frame and to the hands' nodes by ideal kinematic constraints. In particular, the collective lever is connected to the fixed frame by a revolute joint, allowing it to rotate about the global $Y$-axis, pointing towards the pilot's left. It is also connected to the pilot's left hand with a clamp constraint eliminating all the relative degrees of freedom. The cyclic stick is connected to the global frame through a Cardano joint, allowing rotations about the global $X$-axis, pointing towards the helicopter nose, and the global $Y$-axis.

## 3.2 Numerical tests

The $H_{\mathrm{CD}}$, $H_{\mathrm{FDFT}}$, $H_{\mathrm{ADM}^{-1}}$ and $H_{\mathrm{B2FOL}}$ blocks were identified in numerical test performed with the multibody model. The model was generated with biometric characteristics matching the ones of the subject that subsequently took part of the experimental tests. Therefore the model of a female pilot, aged $26$, weighting $53\,\mathrm{kg}$ and $1.72\,\mathrm{m}$ tall has been generated.

Each test, described in detail in the following sections, has been performed through a dedicated MBDyn simulation. MBDyn allows for the automatic execution of stepped-sine identification tests by means of the `harmonic excitation` element, available in the `hfelem` module[2] [11]. The element generates the appropriate sinusoidal signal to be applied as the excitation term, and allows to define a set of signals to be monitored during the simulation. When the frequency and the amplitude of the monitored signals stabilizes (within a user-specified tolerance), the element stores the signal properties (amplitude, phase) and switches to the next defined frequency and amplitude for the forcing term. The integration timestep can be automatically changed to keep constant the number of integration points per period of the excitation signal...

In all the cases presented in this section, the harmonic excitation frequency ranged from $0.5\,\mathrm{Hz}$ to $7.5\,\mathrm{Hz}$, with $0.1\,\mathrm{Hz}$ step. The amplitude was modulated in order to ensure that the system response remained in the linear region.

### 3.2.1 Control device dynamics, $\mathbf{H_{CD}}$

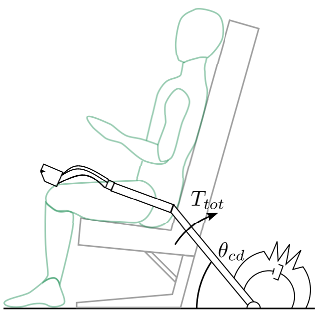


Figure 3: $H_{\mathrm{CD}}$ : lever contribution

To identify $H_{\mathrm{CD}}$ it is necessary to exclude the pilot from the loop (Figure 3). For this reason the joint between the hand and the collective lever has been disabled. The rotation of the lever has been prescribed. In order to do so, a new joint has been established between the lever and the global frame, to mandate the rotational law of the lever once the excitation is imposed. No motion platform acceleration disturbance is present. Once the rotation is prescribed, the moment generated by the constraint to enforce it was extracted from the simulation results, in the form of the reaction moment acting between the global frame and the collective lever, applied to the latter, about the global $Y$ axis. The results obtained from simulation are shown in figure 4.

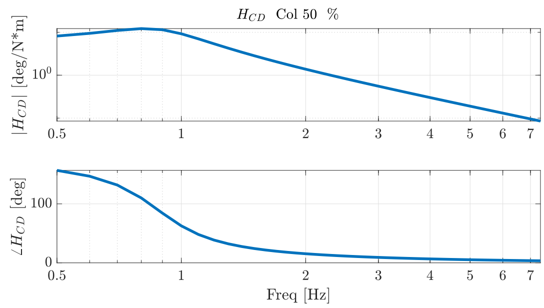


Figure 4: $H_{\mathrm{CD}}$

### 3.2.2 Force dynamics feedthrough, $\mathbf{H_{FDFT}}$

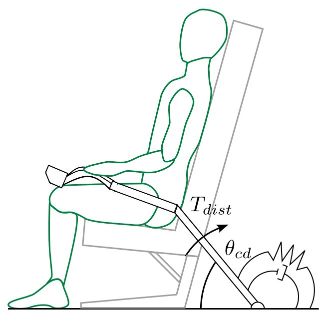


Figure 5: $H_{\mathrm{FDFT}}$: lever and pilot contribution

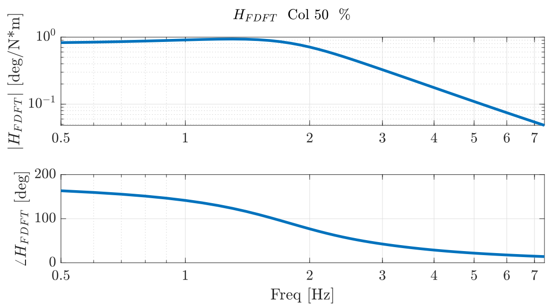


Figure 6: $H_{\mathrm{FDFT}}$

In the definition of the force dynamics feedthrough, $H_{\mathrm{FDFT}}$, both the pilot and the lever are involved (Figure 5).

[2] `https://www.mbdyn.com/Documentation/FAQ.html#what-are-run-time-loadable-modules-and-how-do-they-work`

Indeed, the term is the combination of $H_{\text{CD}}$ and $H_{\text{ADM}}$ as described by equation 4. To obtain this transfer function with the multibody model, a torque was applied to the lever, and the rotation of the lever was extracted. In this case, the pilot is holding the lever: the biomechanical response of the body thus participates in the lever response. The disturbance in platform acceleration is not active. The result is depicted in Figure 6.

#### 3.2.3 Biodynamic feedthrough to forces in open loop, $\mathbf{H_{B2FOL}}$

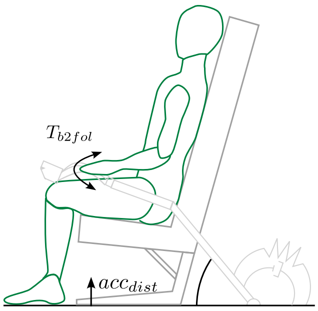


Figure 7: $H_{\text{B2FOL}}$: pilot contribution.

The biodynamic feedthrough to force in open loop, $H_{\text{B2FOL}}$ is solely influenced by the pilot biomechanics (Figure 7). In fact, the definition of the transfer function is

$$H_{\text{B2FOL}} = \frac{T_{\text{b2fol}}(s)}{a_{\text{dist}}(s)} \tag{10}$$

where $T_{\text{b2fol}}$ is the moment generated on the control device by the reaction forces and moments exchanged between the pilot's hand and the control device itself, when it is locked in place. It is important to note that one can conclude that this term depends solely on the pilot if, as in the examined case, the dynamics of the elements connecting the pilot to the base and the pilot to the lever are negligible. In other words, the influence of vertical structural dynamics of the seat, comprising the cushion, and that of the control device grip, must be negligible in frequency range of interest. To calculate $H_{\text{B2FOL}}$, the lever was fixed to prevent rotation, and a vertical disturbance signal $a_{\text{dist}}$ was applied to the platform acceleration. Subsequently, the input ($a_{\text{dist}}$) and output ($T_{\text{b2fol}}$) of the transfer function $H_{\text{B2FOL}}$ were obtained from a stepped sine test. Also in this case, the reaction moment between the hand and the lever was exploited to determine the output (Figure 8).

#### 3.2.4 Neuromuscular admittance, $\mathbf{H_{ADM}}$

The neuromuscular admittance, as the name suggests, involves only the pilot biomechanical response (Figure 9).

In the numerical test, the input signal is represented by a torque applied to the control device. The rotation of the lever $\theta_{\text{cd}}$ (output of $H_{\text{ADM}}$) and the torque $T_{\text{nms}}$ (input) were

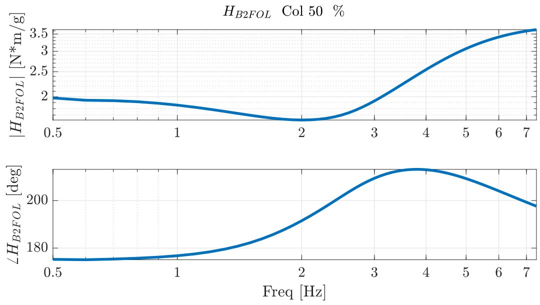


Figure 8: $H_{\text{B2FOL}}$

extracted. To output $T_{\text{nms}}$ has been extracted from the reaction of the joint between the hand and the lever. In this simulation there is no motion platform acceleration disturbance. (It can also be emphasized that this term can be calculated using the relationship in equation 4). The calculated Frequency Response Function (FRF) is shown in figure 10.

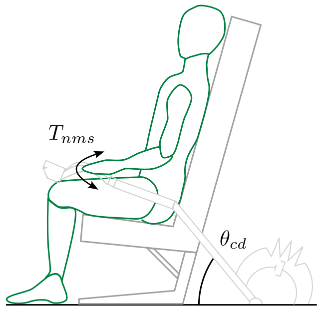


Figure 9: $H_{\text{ADM}}$ : pilot contribution

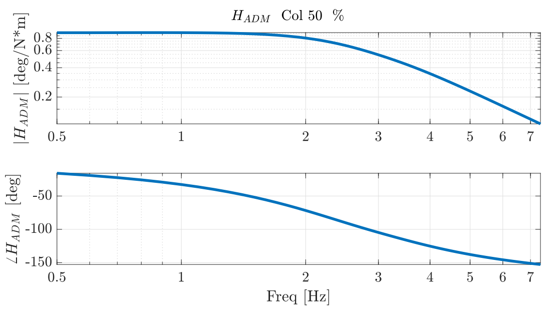


Figure 10: $H_{\text{ADM}}$

### 3.3 Biodynamic Feedthrough, $\mathbf{H_{BDFT}}$

As a mean of verification, the BDFT has been directly estimated in a further numerical test.

To estimate the FRF associated to the biodynamic feedthrough $H_{\text{BDFT}}$, an input in platform vertical acceleration $\ddot{z}$ (representing $a_{\text{dist}}$ in this case), was applied by prescribing the motion of the seat node, through the `harmonic`

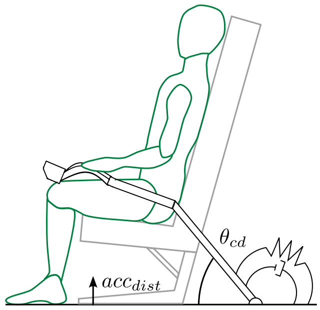


Figure 11: $H_{\text{BDFT}}$: lever and pilot contribution.

excitation element. The rotation of the lever $\theta_{\text{cd}}$, output of $H_{\text{BDFT}}$, was extracted (Equation 1) through the rotation of the node associated the lever rigid body. The resulting direct estimation of $H_{\text{BDFT}}$ is presented in section 4, in Figure 16, compared to the outcome obtained from its reconstruction using the various terms described earlier through equation 2.

### 3.4 Experimental Approach

After exploiting the multibody model for the $H_{\text{BDFT}}$ decomposition process, it was decided to reproduce the process experimentally to validate the results obtained through the numerical approach. Consequently, the various terms necessary for the reconstruction of the $H_{\text{BDFT}}$ were identified experimentally. The experiments were conducted using the RPC testbed, based on a 6-DOF motion platform system, available in the Department of Aerospace Science and Technology laboratories at Politecnico di Milano (Cf. Figure 12) and described in detail in [12]. The testbed

Figure 12: The RPC testbed, at Politecnico di Milano DAER laboratories.

is equipped with a completely reconfigurable helicopter cockpit mockup, mechanical systems simulating the control chain of the collective, cyclic levers and pedals. As mentioned above, this study exclusively investigated the phenomena affecting the collective lever.

A collective lever mockup was constructed with length, mass, and moment of inertia reported in Table 1. Taking into account the ergonomics of

| Parameter | Symbol | Value | Units |
|---|---|---|---|
| Length | $\ell$ | 500.000 | mm |
| Mass | $m_\ell$ | 3.776 | kg |
| CG position | $x_{\text{CG}}$ | 320.000 | mm |
| Reference Position (50%) | $\theta_{0,\text{ref}}$ | 22.000 | ° |
| Moment of inertia w.r.t. CG | $J_\ell$ | 0.092 | $\text{kg}\,\text{m}^2$ |
| Balancing spring constant | $k$ | 1500.000 | $\text{N}\,\text{m}^{-1}$ |
| Balancing spring offset | $r$ | 65.000 | mm |

Table 1: Collective lever mockup characteristics

It was necessary to correctly replicate the balancing system, to ensure that the lever remained in the desired position throughout the experiments. A linear spring, which, when appropriately tensioned, could maintain the lever in the required position, was employed (Cf. Figure14). (The spring's elastic coefficient was measured in the laboratory with a tensile test). With this setup, the experimental trials were performed. Specifically, the following components were experimentally measured: $H_{\text{CD}}$, $H_{\text{B2FOL}}$, $H_{\text{FDFT}}$, $H_{\text{BDFT}}$. No direct test has been performed to identify the neuromuscular admittance, $H_{\text{ADM}}$. Instead, it has been decided to obtain it from the force dynamics feedthrough, $H_{\text{FDFT}}$, and the control device dynamics $H_{\text{CD}}$. The following sections will provide a more detailed explanation of the tests conducted for each term.

#### 3.4.1 Control device dynamics, $\mathbf{H}_{\text{CD}}$

The first tests aimed at identifying $H_{\text{CD}}$, which exclusively depends on the lever dynamics, therefore the pilot is not touching it during the tests. For the identification, it is necessary to apply a torque to the lever and measure its rotation. The test setup used for this experiment is shown in the figures 13 and 14. To apply the torque, an inertial shaker was used. The figures show the shaker mounted on a bracket to reach the desired acting position, which is represented by a crank installed on the collective axis. Connected to the shaker is a stinger made of nylon, equipped with an uniaxial load cell (Piezotronics 208B01). The collective rotation is measured via a Hall effect encoder (Active Sensors MHR5500). Tests are conducted utilizing a Siemens Simcenter SCADAS system, which controls in closed loop the voltage supply to the shaker by evaluating the force measured by the load cell.

Once activated, the shaker moves the stinger, which, being constrained to the lever's feedback system via the load cell, produces a rotation of the lever measured through an encoder. Using the MIMO FRF acquisition procedures of Testlab [13], the test can be conducted, specifically using a random signal as input to the shaker in the frequencies of interest $0.5–7.5\,\mathrm{Hz}$. The frequency resolution was set at $0.1\,\mathrm{Hz}$, with each individual record having a width of $10\,\mathrm{s}$. Subsequently, the FRF was calculated, with the input being the torque applied to the lever and the output being the lever's rotation. The software employs an $H_v$ estimator, which is defined ad the geometric mean of the $H_1$ and $H_2$ estimators:

$$H_1(j\omega) = \frac{S_{f\theta}(j\omega)}{S_{ff}(j\omega)} \tag{11a}$$

$$H_2(j\omega) = \frac{S_{ff}(j\omega)}{S_{\theta f}(j\omega)} \tag{11b}$$

$$H_v = (H_1(j\omega)H_2(j\omega))^{-1/2} \tag{11c}$$

with $S_{ff}(j\omega)$ begin the autospectrum of the input and $S_{f\theta}(j\omega)$ the cross-spectrum of the output with respect to the input. The power spectra were calculated following Welch's algorithm [14], using $60$ averages.

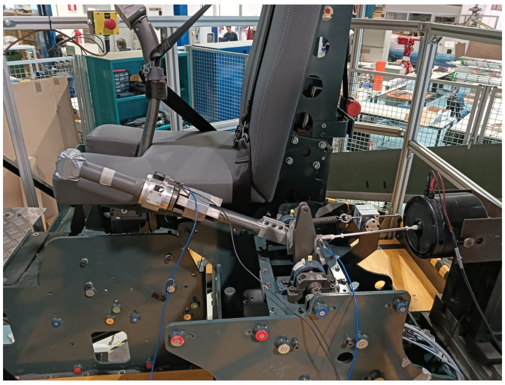

Figure 13: test bed for $H_{\mathrm{CD}}$

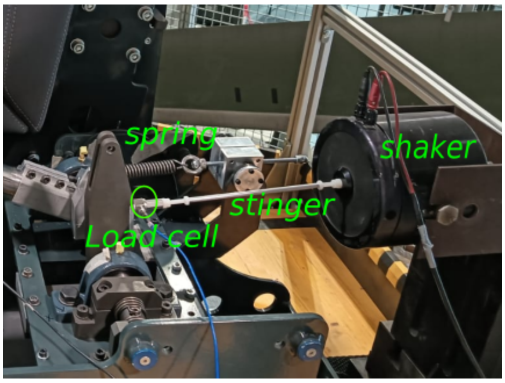


Figure 14: Detail of test bed for $H_{\mathrm{CD}}$: spring, shaker, load cell, stinger

#### 3.4.2 Force dynamics feedthrough, $\mathbf{H_{FDFT}}$

To measure $H_{\mathrm{FDFT}}$, the test setup employed is the same as the one described in the previous paragraph for $H_{\mathrm{CD}}$. In this case, it is also necessary to apply a torque to the lever and measure its rotation. However, unlike before, the pilot is included in the loop. The $H_{\mathrm{FDFT}}$ term describes the pilot-lever system, therefore, the pilot was asked to hold the lever throughout the entire experiment. The input signal to the shaker was, as for $H_{\mathrm{CD}}$, a random signal within the frequency band $0.5–7.5\,\mathrm{Hz}$. The FRF was calculated following the same process described for $H_{\mathrm{CD}}$, with the input being the torque applied to the lever and the output being the lever's rotation.

#### 3.4.3 Biodynamic feedthrough to forces in open loop, $\mathbf{H_{B2FOL}}$

The $H_{\mathrm{B2FOL}}$ term exclusively describes the pilot, when the system is excited through the acceleration disturbance. The input of this term is the platform acceleration, and the moment generated around the pivot point of the lever by the force exchanged between the hand and the lever represents the output. As proposed by Venroij et al. in [2] and mentioned in previous paragraphs, calculating $H_{\mathrm{B2FOL}}$ requires blocking the lever rotation and measuring the force exchanged between the hand and the lever.

A six-axis load cell (Model 6ADF80) was mounted between the lever and the grip as shown in figure 15, and an accelerometer was placed under the seat to measure the input acceleration. To conduct the test, an acceleration disturbance – a white noise signal – was generated through the platform motion control, at the frequencies of interest $0.5–7.5\,\mathrm{Hz}$, and the pilot was asked to hold the lever, maintaining the initial reference rotation $\theta_{\mathrm{ref}}$. A graphical user interface displaying the current and desired control level position was visualized in front of the pilot, on dedicated monitors (for more details, refer to [12]). Using the time data acquisition module of `Testlab`, the data were collected and then analyzed in the frequency domain to obtain the desired FRF.


Figure 15: Load cell between lever and grip

#### 3.4.4 Biodynamic Feedthrough, $H_{\mathrm{BDFT}}$

The $H_{\mathrm{BDFT}}$ term integrates the various contributions describing both the lever and the pilot. To experimentally obtain this term, it is necessary to apply an acceleration to the MPS, identical to the one used for $H_{\mathrm{B2FOL}}$, (measured by the accelerometer under the seat) and measure the rotation of the lever, with the pilot in the loop. The procedure follows the standard one applied to pilot-vehicle systems on the RPC testbed, with more details available in [12].

# 4 Results and Discussion

Numerical and experimental tests have been conducted to identify the constituent blocks of $H_{\text{BDFT}}$, and the resultant $H_{\text{BDFT}}$ obtained from direct numerical tests has been effectively reconstructed through a combination of these blocks. As noted in the previous section, an analytical approach has been employed to estimate $H_{\text{CDFT}}$, for both the experimental and the numerical approaches, yielding satisfactory results particularly when linear models of the main components in the control chain are considered adequate approximations of their real counterparts.

The results obtained with the numerical approach using the multibody model are shown in Figure 16. The blue curve represents the $H_{\text{BDFT}}$ reconstruction obtained following equation 2, while the red dashed curve shows the $H_{\text{BDFT}}$ obtained from experiments. The curves are very close to each other, leading to the conclusion that the decomposition proposed by Venroji et al. [2], which was originally verified for a sidestick configuration, yields satisfactory results also for a helicopter lever (in this case a collective lever). After testing the process on a multibody numerical model and obtaining satisfactory results, the procedure was repeated experimentally. The experimental process proved to be more complex and challenging. Not all terms calculated numerically were subsequently identified experimentally: in particular, the neuromuscular admittance $H_{\text{ADM}}$, for which the experimental setup is challenging because of the need to eliminate the effects of the lever dynamics, while allowing its motion. As an alternative approach, $H_{\text{FDFT}}$ was calculated, allowing the reconstruction to proceed following equations 4 and 2. The results obtained are shown in Figure 17, where the green curve represents the $H_{\text{BDFT}}$ obtained from a direct test, while the yellow curve represents the curve combining the single components. The result is satisfactory. The two curves are close, especially up to a frequency of 4 Hz. At higher frequencies, it can be observed that the $H_{\text{BDFT}}$ obtained directly rises and falls as if another couple of complex conjugated poles was present, a feature that is not well captured by the reconstructed $H_{\text{BDFT}}$. This behavior is likely due to the effect of the first axial mode of the spine, which is typically located in the range $4.5$–$6.5\,\text{Hz}$ and can affect the transmissibility of vertical vibrations from the base to the shoulder girdle[15]. This effect is the subject of further investigations, currently ongoing.
Despite these minor differences, it can be concluded that the process of separately identifying the pilot and lever contributions to the overall biodynamic feedthrough.

It is worth to emphasize the significance of experimental tests, as they are crucial for validating the numerical model. Having a robustly validated numerical model allows for varying the lever and pilot parameters without needing to repeat the experimental procedure.

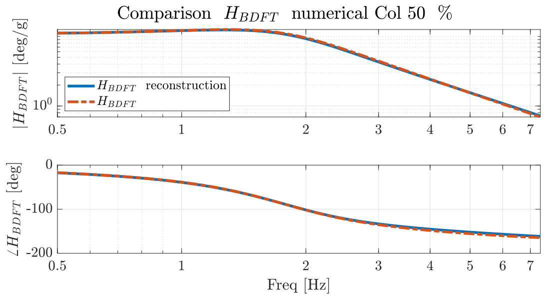


Figure 16: Comparison between the $H_{\text{BDFT}}$ obtained by direct numerical test and through the reconstruction from its components.

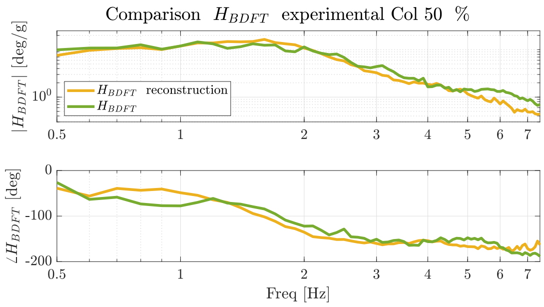


Figure 17: Comparison between the $H_{\text{BDFT}}$ obtained by direct experimental test and through the reconstruction from its components.

For this reason, the results obtained from the experimental $H_{\text{BDFT}}$ were compared with the numerical $H_{\text{BDFT}}$. The results are shown in Figure 18, where the green curve represents the experimental results, and the red curve represents the numerical simulation results. Looking at the magnitude plot, it can be seen that the red curve reproduces the overall trend and absolute value of the green curve. As mentioned in previous analyses, the experimental $H_{\text{BDFT}}$ also shows the presence of a possible additional poles, probably related to the first axial mode of the pilot spine, the effect of which is not currently adequately captured by the numerical model. Also in this case, focus is currently being placed on updating the multibody model to better catch this effect.

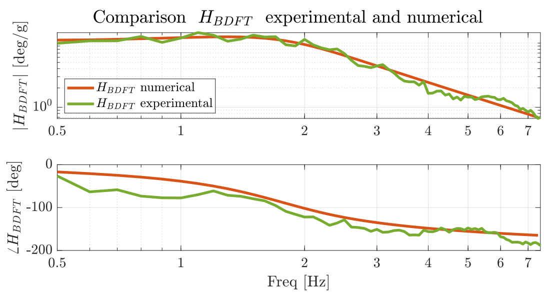


Figure 18: Comparison between the $H_{\text{BDFT}}$ obtained by direct numerical test and the $H_{\text{BDFT}}$ obtained by experimental test .

### 4.1 Conclusions and Future Developments

In this work, the biodynamic feedthrough related to the transmissibility of vibrations between the vertical acceleration of the pilot seat to the rotation of the collective lever, $H_{\mathrm{BDFT}}$, has been decomposed into terms that describe separately the pilot and the lever contributions, an approach adopted from Venrooij's work [2]. This breakdown allows to understand the respective influences of the lever and the pilot in the Biodynamic Feedthrough. Departing from the literature proposals, the control device used in this study is the collective lever of a helicopter. In this study, two distinct approaches were employed: a numerical approach using a detailed multibody model of the upper body and the collective lever, and an experimental approach involving the RPC testbed available at the Politecnico di Milano laboratories. Both methods proved to be satisfactory, leading to the conclusion that the approaches proposed in the literature are viable in the examined case. It is important to stress that these approaches should not be viewed as separate but rather used concurrently. The experimental approach is essential for validating the multibody model. This work represents a preliminary step toward robust model validation.

The results obtained pave the road for numerous future developments. The experimental procedure will be repeated for multiple individuals of different sex, age, height, and weight. This will allow us to test the model's predictability for people with varying biometric characteristics. The multibody model can then be used to perform a comprehensive sensitivity analysis by varying the parameters that describe the lever and those that describe the pilot. This will enable to better understand how each element affects the biodynamic feedthrough, and thus to better support robust design processes for helicopter flight controls.

# 5 References

# References


[1] M. D. Pavel, M. Jump, B. Dang-Vu, *et al.*, "Adverse rotorcraft pilot couplings—Past, present and future challenges," en, *Progress in Aerospace Sciences*, vol. 62, pp. 1–51, Oct. 2013, ISSN: 03760421. DOI: 10.1016/j.paerosci.2013.04.003. [Online]. Available: https://linkinghub.elsevier.com/retrieve/pii/S0376042113000316 (visited on 12/12/2020).

[2] J. Venrooij, D. A. Abbink, M. Mulder, *et al.*, "A Biodynamic Feedthrough Model Based on Neuromuscular Principles," en, *IEEE Transactions on Cybernetics*, vol. 44, no. 7, pp. 1141–1154, Jul. 2014, ISSN: 2168-2267, 2168-2275. DOI: 10.1109/TCYB.2013.2280028. [Online]. Available: http://ieeexplore.ieee.org/document/6594822/ (visited on 10/27/2022).

[3] J. Venrooij, M. Olivari, and H. H. Bülthoff, "Biodynamic Feedthrough: Current Status and Open Issues," en, *IFAC-PapersOnLine*, vol. 49, no. 19, pp. 120–125, 2016, ISSN: 24058963. DOI: 10.1016/j.ifacol.2016.10.472. [Online]. Available: https://linkinghub.elsevier.com/retrieve/pii/S2405896316320626 (visited on 12/12/2020).

[4] A. Zanoni, A. Cocco, and P. Masarati, "Multibody dynamics analysis of the human upper body for rotorcraft–pilot interaction," *Nonlinear Dynamics*, vol. 102, no. 3, pp. 1517–1539, 2020, Type: Article. DOI: 10.1007/s11071-020-06005-7. [Online]. Available: https://www.scopus.com/inward/record.uri?eid=2-s2.0-85094129252&doi=10.1007%2fs11071-020-06005-7&partnerID=40&md5=1f3a327521e3af7d0fdc5743448ece81.

[5] J. Venrooij, D. A. Abbink, M. Mulder, M. M. van Paassen, and M. Mulder, "A method to measure the relationship between biodynamic feedthrough and neuromuscular admittance," *IEEE Transactions on Systems, Man, and Cybernetics, Part B: Cybernetics*, vol. 41, no. 4, pp. 1158–1169, 2011, doi:10.1109/TSMCB.2011.2112347.

[6] P. Masarati, M. Morandini, and P. Mantegazza, "An efficient formulation for general-purpose multibody/multiphysics analysis," vol. 9, no. 4, p. 041 001, 2014, doi:10.1115/1.4025628.

[7] A. Zanoni, A. Cocco, and P. Masarati, "Multibody dynamics analysis of the human upper body for rotorcraft–pilot interaction," vol. 102, no. 3, pp. 1517–1539, 2020, doi:10.1007/s11071-020-06005-7.

[8] E. Pennestrì, R. Stefanelli, P. P. Valentini, and L. Vita, "Virtual musculo-skeletal model for the biomechanical analysis of the upper limb," vol. 40, no. 6, pp. 1350–1361, 2007, doi:10.1016/j.jbiomech.2006.05.013.

[9] K. Saul, W. Murray, and S. Delp, "A model of the upper extremity for simulating musculoskeletal surgery and analyzing neuromuscular control," *Annals of biomedical engineering*, vol. 33, pp. 829–40, Jul. 2005. DOI: 10.1007/s10439-005-3320-7.

[10] P. Masarati, G. Quaranta, and A. Zanoni, "Dependence of helicopter pilots' biodynamic feedthrough on upper limbs' muscular activation patterns," vol. 227, no. 4, pp. 344–362, Dec. 2013. DOI: 10.1177/1464419313490680.

[11] MBDyn Developers, *Mbdyn input file format (input manual)*, 2024, ch. B.1.7.

[12] A. Zanoni, "Experimental test-bed for the identification of biodynamic feedthrough of helicopter-pilot systems," in *48rd European Rotorcraft Forum, ERF 2022*, Winterthur, Switzerland, Sep. 2022.

[13] Siemens, *Simcenter testlab mimo frf testing*, 2023. [Online]. Available: docs.sw.siemens.com.

[14] P. Welch, "The use of fast fourier transform for the estimation of power spectra: A method based on time averaging over short, modified periodograms," *IEEE Trans. Audio Electroacoust.*, vol. 15, no. 2, pp. 70–73, Jun. 1967.

[15] N. J. Mansfield and M. J. Griffin, "Non-linearities in apparent mass and transmissibility during exposure to whole-body vertical vibration," en, *Journal of Biomechanics*, vol. 33, no. 8, pp. 933–941, Aug. 2000, ISSN: 00219290. DOI: 10.1016/S0021-9290(00)00052-X. [Online]. Available: https://linkinghub.elsevier.com/retrieve/pii/S002192900000052X (visited on 07/11/2024).